Soft Matter

PAPER

View Article Online
View Journal | View Issue

Check for updates

Cite this: *Soft Matter*, 2018, **14**, 2655

Tough high modulus hydrogels derived from carbon-nitride *via* an ethylene glycol co-solvent route†

Baris Kumru,[a] Valerio Molinari,[a] Menny Shalom, *[ab] Markus Antonietti[a] and Bernhard V. K. J. Schmidt *[a]

Received 31st January 2018,
Accepted 11th March 2018

DOI: 10.1039/c8sm00232k

rsc.li/soft-matter-journal

High concentration formulations of graphitic carbon nitride (g-CN) are utilized as photoinitiator and reinforcer for hydrogels. In order to integrate significant amounts of g-CN, ethylene glycol (EG) is employed as a co-solvent for the gel formation, which enables stable dispersion of up to 4 wt% g-CN. Afterwards, EG can be removed easily *via* solvent exchange to afford pure hydrogels. The diverse gels possess remarkably high storage moduli (up to 650 kPa for gels and 720 kPa for hydrogels) and compression moduli (up to 9.45 MPa for 4 wt% g-CN EG gel and 3.45 MPa for 4 wt% g-CN hydrogel). Full recovery without energy loss is observed for at least 20 cycles. Moreover, gel formation can be performed in a spatially controlled way utilizing photomasks with desired shapes. Therefore, the suggested method enables formation of hybrid gels by optical lithography with outstanding mechanical properties very similar to natural cartilage and tendon, and opens up opportunities for future applications in photocatalysis, additive manufacturing of biomedical implants and coating materials.

Open Access Article. Published on 13 March 2018. Downloaded on 7/23/2025 12:29:56 PM.
This article is licensed under a Creative Commons Attribution 3.0 Unported Licence.

Introduction

Hydrogels belong to the most studied polymeric materials, which is mainly due to their ability to be composed of significant amounts of water.[1] Hydrogels comprise a soft network structure with high flexibility when they incorporate high amounts of water, but to mimic natural tissues,[2] *e.g.* tendons and cartilages,[3] significant compressive strength beyond the abilities of a simple hydrogel is needed. Materials with high water content but at the same time similar performance as their biological originals could be applied in tissue replacement and repair.[4,5] In addition, various other applications for hydrogels are discussed, *e.g.* as drug delivery agents,[6,7] actuators,[8] and smart materials with self-healing or shape memory properties.[9,10] As already stated, typical hydrogels feature insufficient mechanical strength due to poor distribution of applied stress throughout the polymer network. Therefore, improvement of mechanical properties of hydrogels, mainly through hybrid formation has been a significant interest in recent years.[9,11] Especially addition of fiber-like or plate-like reinforcement agents is a way to enhance mechanical strength *via* a more equal distribution of the applied stress through the network. At the same time, addition of the reinforcing agent increases the crosslinking density resulting in stronger interactions. Common approaches for improvement of hydrogels mechanical properties utilize double network systems,[12–14] nanofibers,[15] tetra armed-PEG crosslinked systems,[16,17] 3D printing,[18] slide-ring gels,[19,20] and introduction of charged supports.[11,21,22] Double network systems are one of the first examples of reinforced hydrogels that consist of a tightly crosslinked first network and a loosely crosslinked secondary network.[12] In such a way good compressive strength could be obtained while keeping a low fatigue resistance at the same time. Nanostructures reinforcing particles provide increased stress dissipation through reinforcer layers, sometimes additionally assisted by charge–charge repulsion between the single sheets.[23] A well-known example is the incorporation of clay that bases on a combination of ionic interaction and hydrogen bonding with polymeric chains, which act as additional crosslinking points.[24] Recently, Aida and coworkers presented negatively charged titanate nanosheets as reinforcer and initiator incorporating inorganic structures into the polymeric network.[25] Moreover, gelation was performed under magnetic field to provide anisotropic microstructures. In a similar approach, we utilized graphitic carbon nitride (g-CN) as reinforcer and polymerization initiator to generate photoactive[26] and strong hydrogels with storage moduli up to 8 kPa at 0.6 wt% reinforcer incorporation.[27]

[a] *Max-Planck-Institute of Colloids and Interfaces, Department of Colloid Chemistry, Am Mühlenberg 1, Potsdam 14476, Germany. E-mail: bernhard.schmidt@mpikg.mpg.de*
[b] *Chemistry Department, Ben Gurion University of the Negev, Beersheba 009728, Israel. E-mail: mennysh@bgu.ac.il*

† Electronic supplementary information (ESI) available. See DOI: 10.1039/c8sm00232k

Open Access Article. Published on 13 March 2018. Downloaded on 7/23/2025 12:29:56 PM.
This article is licensed under a Creative Commons Attribution 3.0 Unported Licence.

g-CN is a highly functional 2D material composed of a polymeric structure *via* repeating tri-*s*-triazine units.[28,29] Due to convenient synthesis from low-cost precursors, good light absorption and tunable properties, g-CN qualifies as a promising (photo)catalytic material.[30] Importantly, g-CN properties, namely surface area, surface electronegativity, surface functionalities and band-gap can be tailored by changing the C/N ratio in the final materials[31] *via* covalent grafting of allyl compounds for enhanced dispersibility[32] or *via* non-covalent modification.[33] Therefore, several prospective applications of g-CNs are discussed, *e.g.* photochemical water splitting,[34,35] CO_2 reduction,[36,37] organic coupling reactions,[38,39] and very recently emulsion stabilization.[40] More close to the present subject, g-CN was utilized in the formation of polymeric materials, *i.e.* as initiator for free radical and controlled photopolymerization reactions[41,42] as well as in the formation of polymer/g-CN composites *via* continuous aerosol method under visible light irradiation.[43] In such a way, monomers like styrene, methyl methacrylate and butyl acrylate were polymerized. Recently, temperature sensitive hydrogels were formed *via* g-CN initiated photopolymerization employing exfoliated g-CN sheets (0.03 wt%) and *N*-isopropylacrylamide (NIPAM).[44] Assembly of g-CN particles with CO_2 as trigger yields reversible hydrogel formation which can be used as dye absorbent.[45] Moreover, reversible hydrogel formation *via* interaction of g-CN layers and ionic liquids was described.[46] Very recently, g-CN was used in the supramolecular hydrogel formation *via* peptide self-assembly through non-covalent interactions.[47] In our earlier report, reinforced hydrogels were formed *via* g-CN with 0.6 wt% loading.[27] In there, mechanical properties of hydrogels were related to the properties of incorporated g-CN. The strength of hydrogel was found to be correlated with the surface charges of g-CN due to the repulsion between the layers upon applied stress. Nevertheless, the effect of g-CN on the mechanical strength was limited in the past due to restricted dispersibility of g-CN in water that arises from strong π–π interactions.[48] On the other hand, it can be expected that increased g-CN content in hydrogel systems will yield significantly stronger materials, which may be applied as rather stiff aquamaterials that act as photoinitiator and photocatalysts at the same time.

Herein, a strategy to improve the mechanical properties of g-CN based hydrogels by the incorporation of a significantly enhanced g-CN content is presented. The high amount of incorporated g-CN in the system is accomplished *via* an approach using ethylene glycol (EG) as co-solvent, which enhances the dispersibility of g-CN in the reaction medium significantly. One pot visible light induced gelation of the mixture is applied to yield tough EG hybrid gels *via* photopolymerization of *N*,*N*-dimethylacrylamide (DMA) and *N*,*N*-methylenebisacrylamide (MBA) (Scheme 1). The EG additive can be removed *via* washing with deionized water to yield pure hydrogels. Both gel types, EG hybrid and hydrogels, are characterized regarding their mechanical properties (rheology and compression) and swelling behavior. Moreover, gels can be formed in soaked tissues and under spatial control. Thus, photo patterned structures can be obtained *via* utilization of photomasks.

Experimental part

Materials

Al_2O_3 basic (Sigma Aldrich), ascorbic acid (AscA, 99%, Sigma Aldrich), cyanuric acid (98%, Sigma Aldrich), ethylene glycol (EG, 99%, Fluka), hydrogen peroxide (30% in water, Sigma Aldrich), melamine (99%, Sigma Aldrich), *N*,*N*-methylenebisacrylamide (MBA, 99%, Sigma Aldrich), Pluronic F127 (Sigma Aldrich), Triton X 305 solution (70 wt% in water, Sigma Aldrich) were used as received. *N*,*N*-Dimethylacrylamide (DMA, 99%, TCI) was passed through basic alumina column prior to use. Tissue paper samples were cut from Kimtech Science brand tissue paper. 50 W LED chips (Foxpic High Power 50 W LED Chip Bulb Light DIY White 3800LM 6500 K) were connected to a self-made circuit and cooling system. g-CN was prepared by using cyanuric acid–melamine complex as precursor according to the literature.[49]

Exemplary synthesis of g-CN derived DMA gels with EG (2 wt% g-CN). 4.5 g deionized water, 4.5 g EG and 200 mg of g-CN (2 wt%) were mixed in a plastic centrifuge tube. The mixture was ultrasonicated at 50% amplitude for 40 minutes (2 minute portions, 20 times) to yield a dispersion. Subsequently, the dispersion was transferred into a 20 mL glass vial, 0.8 g DMA (8 wt%) and 0.06 g MBA (0.06 wt%) were added. Nitrogen was flushed through the system for 3 minutes and the vial was capped. The mixture was put between two 50 W LED daylight sources (20 cm apart from each other) to initiate gelation. Gelation was completed in 30 minutes, the gel was removed from the vial and put into 40 mL deionized water for 2 hours for purification.

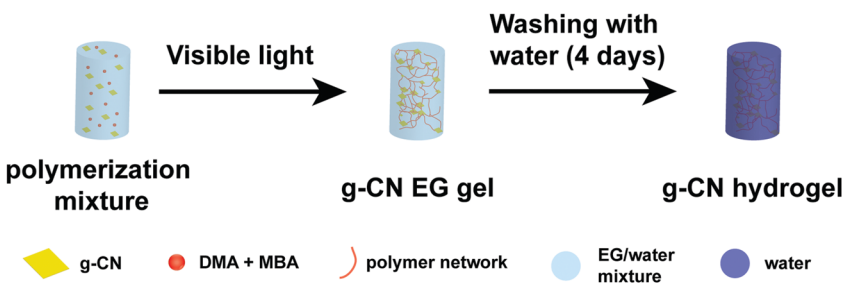

Scheme 1 Overview for EG gel formation *via* visible light irradiation and washing of hybrid gel network to obtain pure hydrogels (DMA: *N*,*N*-dimethylacrylamide; MBA: *N*,*N*-methylenebisacrylamide; EG: ethylene glycol).

 This journal is © The Royal Society of Chemistry 2018

Open Access Article. Published on 13 March 2018. Downloaded on 7/23/2025 12:29:56 PM.
This article is licensed under a Creative Commons Attribution 3.0 Unported Licence.

Removal of EG from EG gel samples. All EG gel samples with different g-CN concentrations were immersed in 100 mL deionized water. The gels were kept in the water for 4 days and the water was exchanged 3 times a day.

Freeze drying of hydrogel samples. After standing in distilled water for 4 days; the hydrogels were cut into smaller pieces, transferred into a flask and dried by pump thaw cycles until the moisture droplets on the flask were not visible anymore. In this frozen form, they were immediately put into Lyotech GT 2E freeze dryer overnight. Resulting products are rubber-like EG gels or brittle hydrogels which retain their pores on the microscopic level.

Characterization

Zeta potential measurement of colloidal suspension of g-CN was performed with a Zetasizer Nano ZS90 from Malvern. X-Ray diffraction (XRD) patterns were obtained using Bruker D8 Advance X-ray diffractometer *via* Cu-K_α radiation. Scanning electron microscopy (SEM) was performed using JSM-7500F (JEOL) equipped with an Oxford Instruments X-MAX 80 mm^2 detector for the determination of the morphology of g-CN. Fourier transform infrared (FT-IR) spectra were taken on Nicolet iS 5 FT-IR spectrometer. Solid state ultraviolet-visible (UV-vis) spectroscopy was recorded *via* a Cary 500 Scan spectrophotometer equipped with an integrating sphere. Porosimetry was performed using Quantachrome Quadrasorb instrument with N_2 gas after g-CN samples were degassed at 100 °C overnight. Surface area of the g-CN was estimated *via* the Brunauer–Emmett–Teller (BET) method. Thermogravimetric analysis (TGA) was performed *via* TG 209 Libra from Netzsch in nitrogen atmosphere with a heating rate 10 K min^{-1} using aluminum crucible for samples. Remaining EG incorporation after freeze drying was calculated from the mass loss between 120–200 °C (in order to exclude water elimination). Ultrasonication was performed *via* an ultrasonicator at 50% amplitude (Branson D450). Elemental analysis of g-CN was recorded *via* a Vario Micro device. Swelling and rheological analysis of gels and hydrogel samples was performed as follows. To obtain the swelling ratios of gels and hydrogel samples manually 100 mg (W_d) freeze dried gel or hydrogel sample were put into a flask which contains 5 mL distilled water and left to stand for 24 hours. Swollen gels or hydrogels are weighed (W_s) and swelling ratio is calculated by using the formula:

$$\text{Swelling ratio} = \frac{W_s - W_d}{W_d} \times 100\%$$

For rheological investigations, purified and swollen hydrogels (or EG gels after reaction) were cut into small disc shapes and investigated with an Anton Parr MCR 301 rheometer equipped with a cone plate 12 (CP-12). Measurements were performed at constant angular frequency (10 rad s^{-1}) with strain range from 0.1–100% with 31 measuring points and 0.02 mm gap. Frequency dependent measurements were performed at constant strain (0.1%) with changing frequency in the range of 1–100 rad s^{-1}. Cyclic rheology was performed immediately after 1st measurement was completed. The relative error from rheology was estimated to be 2.5%. Compression measurements were measured on a Zwick mechanical tester zwickiLine Z2.5 equipped with a loadcell of 10 N or 1 kN. Measurements were recorded after a preload of 0.1 N (speed pre-load 40 mm s^{-1}) and the test was performed at 0.05 mm s^{-1}. The cycling tests were performed until 6 mm of maximum strain (on specimens of 10 mm in height) before the stress was removed to restart the cycle (20 times). Compression modulus was calculated at 10% of strain before break for every specimen. All the compression measurements were recorded using the software TestXpert II V3.71.

Results and discussion

g-CN properties and dispersibility

In order to conduct photoinitiated gel formation, g-CN was synthesized according to previous reports utilizing cyanuric acid-melamine as precursor.[49] Synthesized g-CN possesses a decent negative surface charge and porosity (Table S1 and Fig. S1, ESI†). As g-CN has low dispersibility in aqueous media, hydrogels with g-CN incorporation above 0.6 wt% were not accessible so far.[27] Addition of surfactants (1 wt%) yields seemingly nice dispersions after ultrasonication for 20 minutes, however sedimentation takes place within 10 minutes for 2 wt% g-CN in water (Fig. S2, ESI†). In order to increase dispersibility of g-CN, utilization of a co-solvent in addition to water was investigated. Addition of common water miscible solvents such as acetone, alcohols and *N*-methyl-2-pyrrolidone had negative effects on g-CN dispersibility leading to immediate precipitation. Interestingly, addition of ethylene glycol (EG) to water in a ratio of 1 : 1 w/w significantly increased the dispersibility of g-CN (Fig. S3, ESI†), while variation in EG : water ratio showed negative effect for the preparation of dispersions (Fig. S4, ESI†). Utilization of pure ethylene glycol as dispersion medium for g-CN was reported in the literature in order to synthesize doped g-CN quantum dots, where experimental investigations reported that upon ultrasonication, C–N bond between melem units break and ethylene glycol acts as radical scavenger, yielding smaller sized particles[50] or recently for the formation of thin g-CN films.[51] A similar effect was reported for hexagonal boron nitride nanosheet dispersions.[52] The reason for enhanced dispersibility is two-fold.[53] First of all, polar solvents are effective in exfoliation of carbon nitride sheets *via* intercalation in the stacked structure and hydrogen bonding. Moreover, an efficient exfoliation can be obtained when surface energy of solvent and carbon nitride are in a similar range, which is the case for EG. The co-solvent approach allows the preparation of dispersions with solid contents of g-CN up to 4 wt%. Higher contents of g-CN led to non-uniform dispersions containing non-dispersed solid particles after ultrasonication (Fig. S5, ESI†). Therefore, dispersions containing 2, 3 and 4 wt% g-CN were prepared *via* ultrasonication for further studies. To avoid side reactions, initial dispersions were prepared without monomer and crosslinker. A visual inspection of the formed dispersion was performed before and after ultrasonication of mixtures (Fig. S3, ESI†) showing uniform dispersions that could be utilized for the photocrosslinking step. The stability of dispersions was confirmed *via* no observation of sedimentation of g-CN particles over 4 hours,

Open Access Article. Published on 13 March 2018. Downloaded on 7/23/2025 12:29:56 PM.
This article is licensed under a Creative Commons Attribution 3.0 Unported Licence.

where sedimentation occurs at g-CN concentrations above 4 wt%. Thus, a maximum of 4 wt% g-CN was added to ensure dispersion throughout hydrogel formation, which is described in the following section.

Photoinitiated gel formation

In the next step, the formed g-CN EG–water dispersions were used for gel formation (Scheme 1). For that, monomer and crosslinker were added, nitrogen was flushed through the mixtures, and polymerization was initiated *via* illumination with two 50 W white LED sources. Due to the photoactivity of g-CN, complete gelations were achieved in less than 1 h. Compared to the literature[26,27] a significantly faster gelation rate was observed that is attributed to the enhanced amount of g-CN in the system. Furthermore, a reference DMA EG gel crosslinked with MBA was synthesized using AscA–H_2O_2 redox couple (1 wt%) as a radical initiator. In order to investigate the mechanical properties, rheology measurements of EG gel samples were performed (Table 1, Fig. 1 and Fig. S6, ESI†), *e.g.* 4% g-CN EG hybrid gel has a remarkable G' value of 645 ± 1.6 kPa at 0.1% strain. In the presence of g-CN, gels show significantly increased G' values due to the reinforcement effect from g-CN when compared to the reference gel (Fig. S7, ESI†). Very typical for such systems, increasing amounts of g-CN improve the G' values at low strain but cause more significant shear thinning at high strains. Frequency dependent rheology measurements in the presence of EG did not show significant change in the region between 0–10 rad s^{-1}, (Fig. S6, ESI†), as well as 4% g-CN EG gel and 4% g-CN hydrogel between 1–100 rad s^{-1} (Fig. 1c).

As discussed previously,[27] the utilization of g-CN as initiator leads to the formation of radicals on its surface and chain growth starts from g-CN surface. Hence, g-CN acts as colloidal crosslinker in the system. In order to study the effect in the co-solvent approach, polymerization was performed for 2% g-CN EG gel system without external crosslinker (MBA) addition. After 4 hours, a highly viscoelastic liquid that has gel character as shown *via* rheology was obtained (Fig. S8, ESI†). For this system G' value of 2.0 ± 0.005 kPa and G'' values of 0.5 ± 0.001 kPa at 0.1% strain were obtained, suggesting that in the presence of EG, g-CN also acts as crosslinker and yields relatively strong gels compared with non-g-CN based reference gel even without addition of a small molecule crosslinker. To confirm the statement, control reactions were performed. Gel formation does not take place in the presence of redox initiator and g-CN in dark but without MBA. This clearly indicates the necessity of light irradiation to form gels *via* attachment of polymeric chains to g-CN. Moreover, redox couple initiation without MBA addition does not yield crosslinked systems, in a similar way as irradiation of just monomer and crosslinker without radical source does not yield a hydrogel. The addition of radical scavengers such as hydroquinone completely inhibits gel formation, which points to the radical mechanism of gel formation. The effect of covalent bonding on reinforcement was investigated *via* performing gelation reactions with related g-CN amounts with redox initiators in dark. Therefore, g-CN remains as unreacted particles buried in the gel network. Dramatic decrease in G' values for all concentrations were observed, up to 98% (Fig. S9, ESI†). Clearly covalent reinforcement plays an important role to yield strong hydrogels. Reaching higher g-CN concentrations and performing gelation with non-dispersed particles significantly decreases G' value of gel compared to dispersed systems, which is an important indication for the importance of dispersed particles on reinforcement (Fig. S10, ESI†).

The removal of EG from hybrid gels was performed *via* solvent exchange as previously reported for other solvents.[54] Hybrid gels were washed with water *via* immersion and frequent solvent exchange, which yields swollen hydrogels in a convenient way. No particles were observed in solution during washing process which hints to a covalent bonding of g-CN and polymeric network. The solvent exchange was monitored *via* FT-IR measurements of freeze-dried samples after various periods of time. Rheology measurements of hydrogels without EG were performed (Fig. S11, ESI†) to assess the effect of EG incorporation on mechanical properties (Table 1). Storage moduli similar to EG gels were obtained, *e.g.* 4% g-CN hydrogel has a G' value of 729 ± 1.8 kPa at 0.1% strain. Again, significant shear thinning behavior was evident as G' values decrease in all samples as strain increases. In any case, the reference DMA hydrogel possesses significantly lower G' values of 0.3 kPa at any strain compared with the g-CN reinforced hydrogels. Redox initiated g-CN hydrogels possess much lower G' and G'' values at any strain, by showing an increase in G' values with increased g-CN concentration (Fig. S12, ESI†). Therefore, strength of hydrogel also depends on the incorporated g-CN amount itself. Overall, covalent incorporation of g-CN in hydrogels provides increased mechanical strength due to reinforcing effect of g-CN, which can be attributed to increased number of mechanically active crosslinking points and an increased repulsion between g-CN layers upon compression. To the best of our knowledge the obtained G' values by incorporation of g-CN

Table 1 Overview of the storage moduli (G') and loss moduli (G'') values of g-CN EG gels and hydrogels at different strain

Sample	G' at 0.1% strain (kPa)	G'' at 0.1% strain (kPa)	G' at 20% strain (kPa)	G'' at 20% strain (kPa)
2% g-CN-EG gel	96.5 ± 0.2	18.1 ± 0.05	11.7 ± 0.03	9.9 ± 0.02
3% g-CN-EG gel	460 ± 1.2	75 ± 0.19	58.1 ± 0.15	41.6 ± 0.10
4% g-CN-EG gel	645 ± 1.6	93.7 ± 0.23	53.2 ± 0.13	45 ± 0.11
2% g-CN hydrogel	88.3 ± 0.2	20.4 ± 0.05	25.8 ± 0.06	20.4 ± 0.05
3% g-CN hydrogel	430 ± 1.1	35.1 ± 0.09	78.4 ± 0.20	45 ± 0.11
4% g-CN hydrogel	729 ± 1.8	74.4 ± 0.19	70.7 ± 0.18	59.7 ± 0.15

 This journal is © The Royal Society of Chemistry 2018

Open Access Article. Published on 13 March 2018. Downloaded on 7/23/2025 12:29:56 PM.
This article is licensed under a Creative Commons Attribution 3.0 Unported Licence.

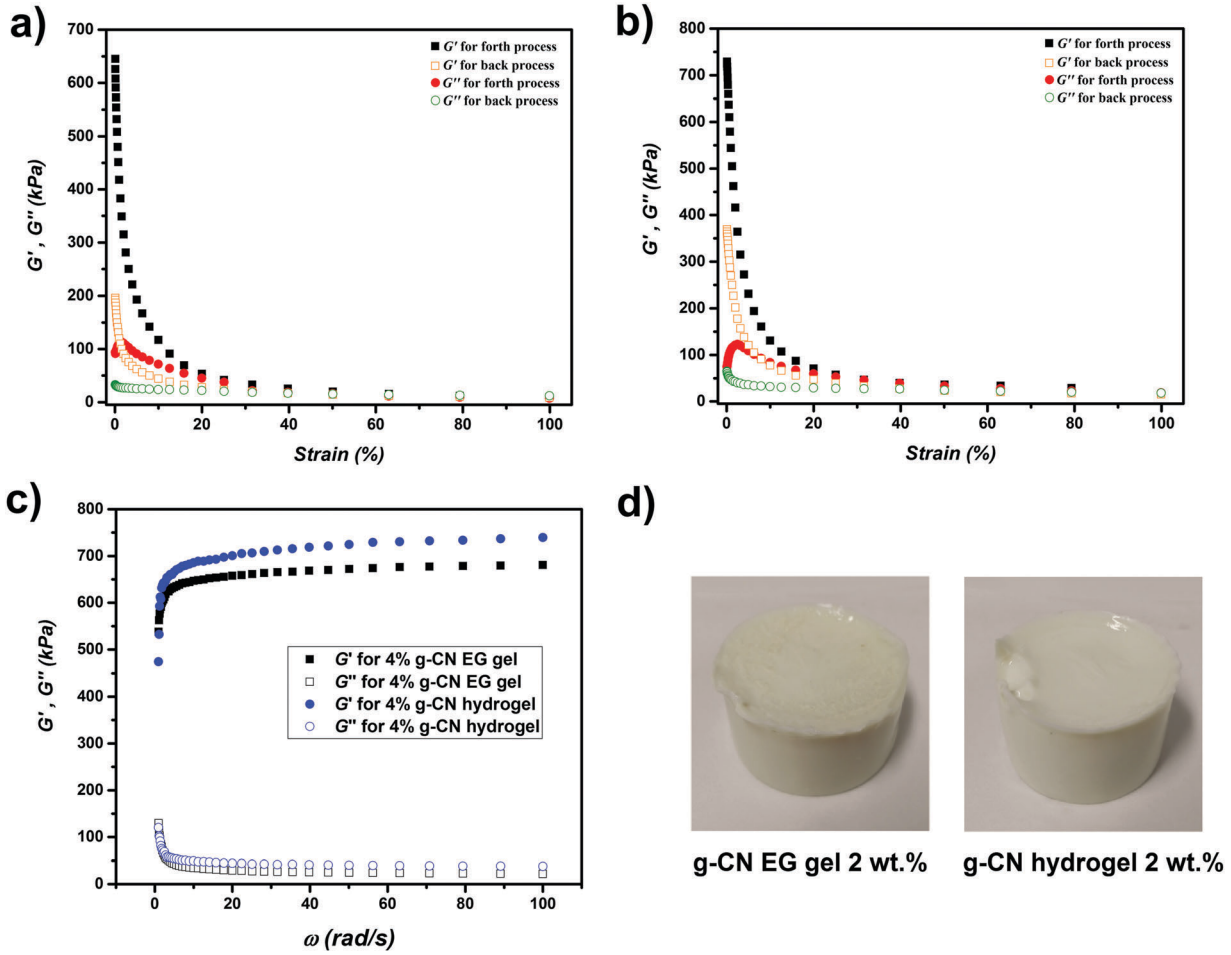

Fig. 1 Comparison of storage (G', black and orange squares) and loss modulus (G'', red and green circles) of (a) 4% g-CN EG and (b) 4% g-CN hydrogel against strain, back (open) and forth (filled) process, (c) G' and G'' values of 4% g-CN EG gel and 4% hydrogel against frequency with constant strain (0.1%) and (d) images of free standing g-CN derived gels.

belong to the highest for reinforced hydrogels reported up to date[55] (a comparison with G' values from literature are presented in Table S2, ESI†).[25,27,56–58]

Decrease of G' with increasing strain is a common effect when inorganic supports are used.[59] The hydrogels are composed of 2 different networks, namely the polymeric network and the inorganic network from sheet–sheet interaction. Upon increased strain, shear-induced deformation of these networks occurs and G' decreases.[60] In particular, sheet–sheet interactions (strong π–π interaction between g-CN sheets due to aromatic repeating units of g-CN)[33] are broken due to the shear stress, leading to alignment of g-CN sheets with the shear flow. Thus, shear thinning is observed. At high g-CN concentration the mechanical properties of the gel increase due to the enhanced sheet–sheet interaction. At the same time more pronounced strain dependency of storage and loss moduli are obtained. The non-linear increase of G' with increasing g-CN content might be due to significantly enhanced sheet–sheet contacts in the gels with higher g-CN amount. Accordingly, the storage modulus rapidly decreases with strain the most for gels with the highest amount of g-CN as the interactions of g-CN is broken due to shear force. In EG hybrid gels, the decrease in G' is more significant than for hydrogels. Moreover, lower G' values were observed for hydrogels compared to EG hybrid gels, which is due to weakened charge dissociation in EG gels. After significant increase of strain, the sheet–sheet interaction network is disturbed and a stable network could not be formed again on the time scale of the back process. A comparison of G' values for both systems at 0.1% and 10% strain shows that except for 4% g-CN systems, EG gels possess higher G' values at very low strains and hydrogels possess higher G' values at higher strains (after around 4% strain) (Fig. S13, ESI†), which can be explained with the decreased charge dissociation and sheet–sheet interactions in EG gels that lead to a stronger strain dependency.

Another property of hydrogels of key importance is compressibility with stress and durability in cyclic compression. Classical hydrogels as soft polymeric networks often fail upon gentle compression due to a loss of mobility of the entanglements of chains and poor distribution of applied stress, and then the broken system is useless in tissue repair. However, reinforced hydrogels are expected to dissipate the stress through the

Open Access Article. Published on 13 March 2018. Downloaded on 7/23/2025 12:29:56 PM.
This article is licensed under a Creative Commons Attribution 3.0 Unported Licence.

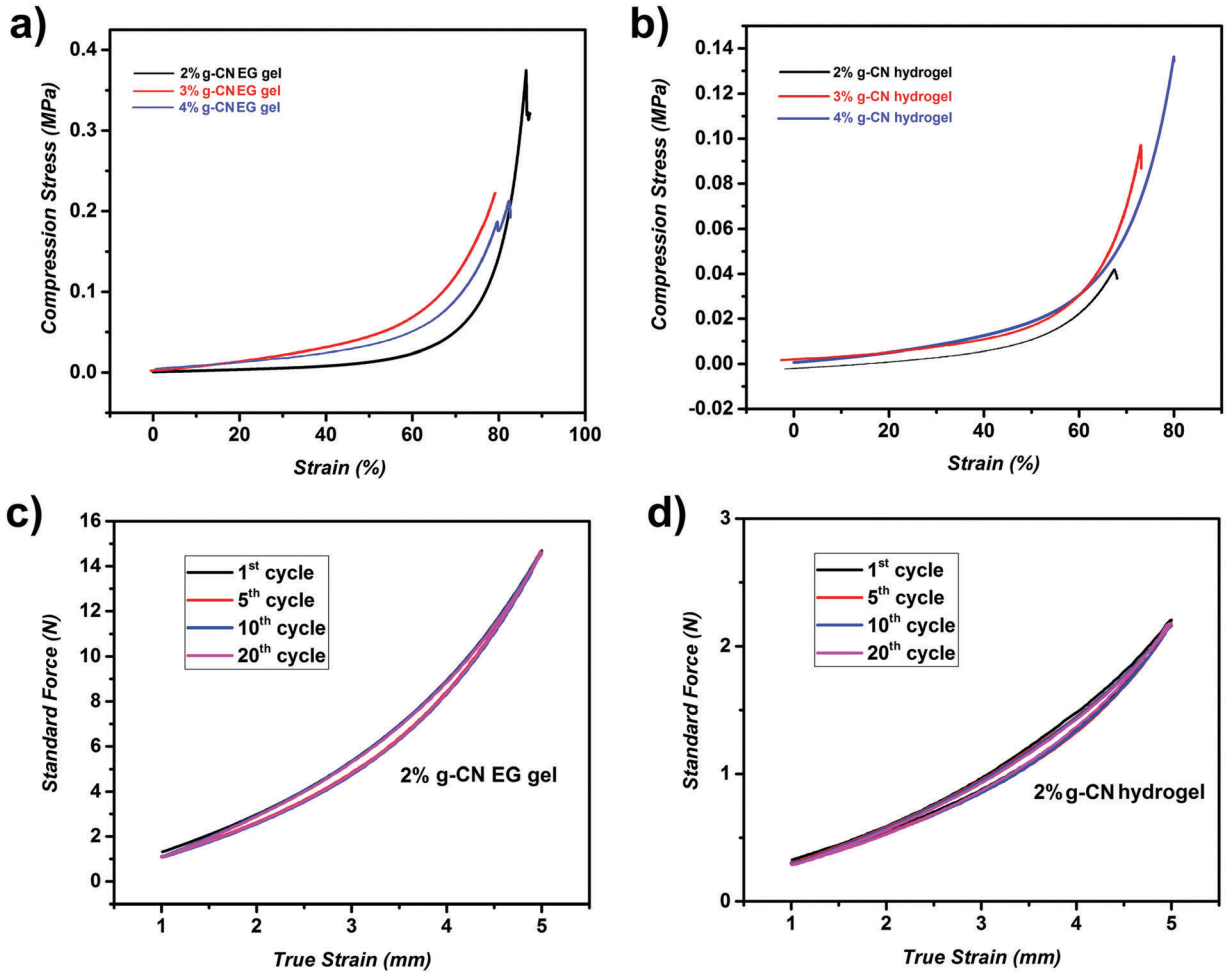

Fig. 2 Compression test results of (a) EG gels and (b) hydrogels and cyclic compression graphs of (c) 2% g-CN EG gel and (d) 2% g-CN hydrogel for 20 cycles.

reinforcer more effectively, and increased compression stress can be usually applied before failure of the crosslinked structure.

g-CN derived hybrid gels and hydrogels show excellent compression properties (Fig. 2 and Table 2). Especially, EG hybrid gels show high elongation at break values, *e.g.* 84% for 2% g-CN EG gel. Moreover, compression tests show that 2% g-CN EG gel possesses the highest compression modulus (E_{mod}) of 9.45 MPa compared to the other EG gel samples. In addition, 2% g-CN EG shows the highest strength in the series with an average fracture stress of 316 kPa. Increased amounts of EG lead to decreased charge dissipation of g-CN sheets, which provides more flexibility to the gels.[61]

As g-CN is covalently bound to the polymer network, no g-CN particle leakage was observed during the washing process. Moreover, g-CN particles incorporation in the gels is indicated *via* UV-vis spectroscopy as discussed in the next section. Another indication for covalent binding is the formation of gels without addition of external crosslinker (MBA). The mechanism of bond

Table 2 Overview of compression test results of EG gels and hydrogels

Sample	Strain at which E_{mod} was calculated[a] (%)	Average E_{mod} (MPa)	Average fracture strain (%)	Average fracture stress (kPa)
2% g-CN-EG gel	72–73	9.45 ± 0.9	84	316 ± 57
3% g-CN-EG gel	71–72	7.70 ± 0.2	81	199 ± 62
4% g-CN-EG gel	64–65	6.45 ± 0.9	74	210 ± 46
2% g-CN hydrogel	56–57	1.27 ± 0.5	67	39 ± 21
3% g-CN hydrogel	56–57	3.10 ± 0.2	66	83 ± 20
4% g-CN hydrogel	58–59	3.55 ± 0.7	68	86 ± 42

[a] E_{mod} was calculated at strain values equal to 10% before break of specimen *via* the slope of the stress–strain curve.

 This journal is © The Royal Society of Chemistry 2018

Open Access Article. Published on 13 March 2018. Downloaded on 7/23/2025 12:29:56 PM.
This article is licensed under a Creative Commons Attribution 3.0 Unported Licence.

formation has been investigated recently.[32] After removal of EG from the system, lower compression moduli and fracture strain values are observed. In contrast to EG gels, the hydrogels show an improvement in compression modulus as g-CN content increases, and the 4% g-CN hydrogel is the strongest hydrogel with 3.55 MPa compression modulus value. Moreover, hydrogels show less strength as indicted by the average fracture stress of 39 to 86 kPa. In comparison, EG gels possess much higher fracture stress and compression modulus values than hydrogels, possibly due to less charge dissipation of g-CN sheets. Absence of EG also results in lower flexibility and causes lower strain at fracture values for hydrogels. Thus, calculation of compression modulus values was performed at different elongations (Table 2). As several samples were investigated to obtain the average result for each sample, compression test results of each sample for EG gels and hydrogels is given in the ESI† (Fig. S14–S19). A comparison of E_{mod} values of gels with literature is presented in Table S3 (ESI†).[3,13,14,62–64]

To investigate the fatigue resistance of EG gels and hydrogels, consecutive cyclic compression tests were performed. Standard force was recorded against true strain, which is the absolute change in plate distance, with an elongation of 50%. A total of 20 compression cycles were conducted for each sample of EG gels and hydrogels. Overall, cyclic compression showed no significant non-recoverable damages for all hybrid gel and hydrogel samples (Fig. 2 and Fig. S20–S23, ESI†). Recovery of the initial strength shows that after compression, alignment of a non-damaged polymeric network and reinforcer was achieved successfully leading to the same behavior as the initial synthesized structures. In comparison with hydrogels, EG gels show higher net force upon compression. Reversible recovery profiles are important for applicability of covalently bound reinforced hydrogels as broken crosslinking points cannot be regenerated after compression. Therefore, it can be concluded that direct covalent bonds between g-CN and polymeric network are strong enough to bear compression at elongations of up to 50%. Moreover, the gels have the capacity to recover their original structure without any energy loss in the system even after 20 consecutive compression cycles. As summary, tough and mechanically stable hydrogels could be formed *via* covalent reinforcement.

As g-CNs are active under visible light, sunlight is also an efficient source to initiate gelation. Hence, a vial containing the polymerization mixture was put outside on a sunny day and during 1 hour gelation was completed (Fig. S24, ESI†) showing the facile approach of g-CN initiated gelation.

Swelling and photophysical properties of g-CN derived gels

The swelling ratio defines the capacity of 3D crosslinked hydrophilic networks for water uptake, which is an important property of hydrogels. Addition of solid reinforcers, such as clays and titanates, lead to decreased water uptake in the system due to hydrophobic interactions.[65] Moreover, increasing number of crosslinks lead to restrictions in the swelling as lengths of chain segments decrease accordingly, which limits elongation of the gel. Hence, a challenging aspect for reinforced hydrogels is the preservation of the swelling property of the material, while enhancing mechanical properties at the same time. In the present case, swelling behavior of gels and hydrogels were calculated *via* using the formula given in experimental section from the masses of dry samples from freeze-drying and swollen samples after immersing dried samples in water (Fig. 3).

After the freeze drying process, EG is still present in the gel network occupying the pores. Quantification *via* TGA of freeze dried g-CN EG gel samples indicates that samples contain around 40 wt% EG after freeze drying (Fig. S25 and Experimental Part, ESI†). Consequently, molecular water uptakes of EG gel samples with respect to the overall weight are expected to be lower than for hydrogel samples due to remaining EG after freeze drying. Thus, swelling ratios of 250 to 150% were

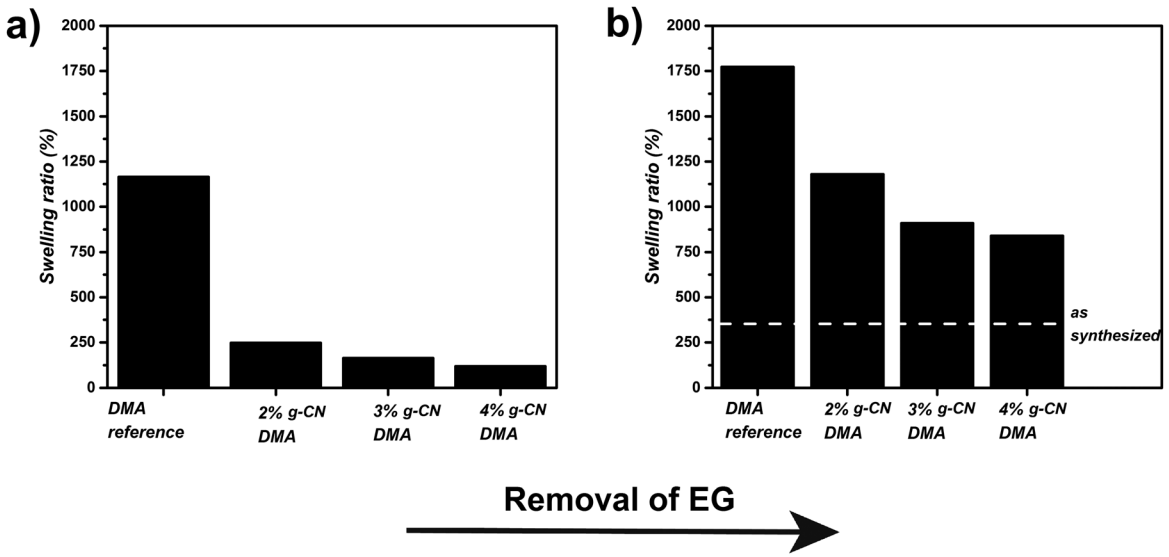

Fig. 3 Swelling ratios at equilibrium in water after 24 hours of (a) EG gels after freeze drying (40% remaining EG) and (b) hydrogels after freeze drying.

Open Access Article. Published on 13 March 2018. Downloaded on 7/23/2025 12:29:56 PM.
This article is licensed under a Creative Commons Attribution 3.0 Unported Licence.

observed for EG gels. In the case of hydrogel samples, higher swelling ratios are obtained, *e.g.* 1100% for 2% g-CN hydrogel. Nevertheless, reference hydrogels show an increased swelling by a factor of 2 compared to g-CN-derived hydrogels as g-CN provides increased crosslinking density.

As g-CN has characteristic absorption bands in the UV-vis range (Fig. S26, ESI†), g-CN derived EG gels and hydrogels show similar absorption profiles which points towards g-CN incorporation in the gels as well as unaltered photophysical properties (Fig. S27, ESI†). FT-IR and XRD methods are also useful to determine the functional group presence and crystalline structures of the samples (Fig. S28 for g-CN, Fig. S29 for g-CN EG gels and Fig. S30 for g-CN hydrogels, ESI†), *e.g.* g-CN shows dominant bands between 1630 and 1250 cm^{-1} in FT-IR which are due to C=N and C–N stretching, respectively. In EG gels and hydrogel samples g-CN characteristic bands are present as well as a band around 1700 cm^{-1} that is due to carbonyl group stretching of the monomers. Moreover, in EG gel samples the existence of strong broad bands around 3200 cm^{-1} are present due to hydroxyl groups of EG, which are almost absent in hydrogel samples. Crystalline profile of g-CN possesses a strong peak in XRD at 27° (Fig. S30b, ESI†), which is clearly observable in EG gel samples as well. However, after EG removal, a large peak formation between 15–30° was observed which is due to amplified sheet–sheet interactions.[66] As already mentioned, EG gels have less dissociated charges, which lead to weakened sheet–sheet interactions. Consequently, sheet–sheet interactions are enhanced after EG removal.

Spatial control over gel formation

As gelation occurs *via* visible light, spatially controlled polymerization was investigated as well, *i.e.* photopatterning (Fig. 4). Illumination of certain parts in the system yields gels with patterned shapes. To illustrate the concept, the polymerization mixture was poured into a plastic dish, covered with a patterned mask and irradiated directly from the top while keeping the temperature of the mixture stable in order to avoid heat-assisted polymerization. In order to evaluate the approach, different patterns were used and partial illumination resulted in desired structures of free standing gels (Fig. 4 and Fig. S31, ESI†). In a half-illuminated system, the illuminated half forms gel and the other half remains liquid. Moreover, symbols from deck of cards were patterned *via* various masks as presented in Fig. 4 and Fig. S31 (ESI†). Further investigation regarding photopatterning was conducted *via* formation of patterned thin gels on the surface of glass slides (Fig. 4).

Another feature is photopolymerization around preformed gels that allows formation of a singular network after a previous gelation. First, a thick gel was created and put into plastic Petri dish, where the dish was filled with monomer mixture around precursor gel network. After gelation was completed, the system yielded a single gel network which can be seen from the difference in thickness (Fig. S32, ESI†). Overall, patterning and formation of single networks after second gelation may be a hint for future applications in additive manufacturing technologies.

In order to broaden the scope of gel formation, the gelation was performed within structure scaffolds with near-medical application profile. Flexible, thin, porous, but robust structures like thin lab tissue paper were utilized as a matrix for gel formation, with the final goal to have a thin sliceable supported hydrogel, *e.g.* for wound coverage. Thus, tissue paper was soaked with the initial EG mixture and treated with visible light. After 1 hour, the tissue paper was taken and washed with deionized water continuously for the removal of unreacted monomers. Finally, a pale yellow tissue was obtained. Under UV light, it is possible to observe fluorescence on the tissue due to g-CN incorporation. In contrast a reference sample tissue remains dark (Fig. S33, ESI†). Such photoactive tissue/hydrogel hybrids might be a promising material for photocatalytic applications like artificial photosynthesis or as antimicrobial surface *via* photocatalytic generation of biocidal reactive oxygen species. Moreover, applications as cartilage or tendon replacement are in reach, as the presented novel materials have compressive moduli in a similar order as mentioned natural tissues,[67,68] *e.g.* storage moduli of 880 kPa and compression moduli of 0.08–2.1 MPa for cartilage. In such a way application as components for intervertebral disc implants are expected, especially when additive manufacturing methods such as 3D printing are utilized. Nevertheless, biocompatibility of the

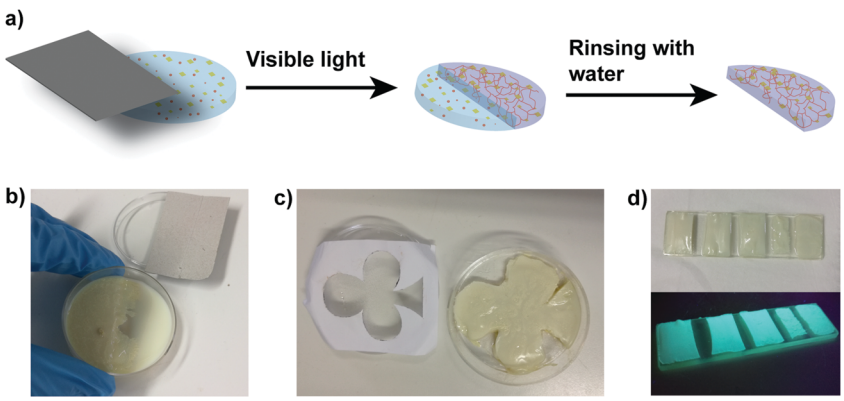

Fig. 4 Spatial control of hybrid gel formation: (a) schematic overview, (b) formation of a self-standing half-circle after rinsing with water, (c) formation of a self-standing club shape after rinsing with water and (d) photopatterning of stripes on a glass slide after rinsing with water.

 This journal is © The Royal Society of Chemistry 2018

Open Access Article. Published on 13 March 2018. Downloaded on 7/23/2025 12:29:56 PM.
This article is licensed under a Creative Commons Attribution 3.0 Unported Licence.

formed hydrogels has to be assessed in order to facilitate biology or medicine related applications.

Conclusions

This contribution described a procedure how significantly increased amounts of g-CN nanosheets (up to 4 wt%) could be stabilized in aqueous monomer mixtures to form hybrid hydrogels. The g-CN can subsequently be utilized as photo-initiator and reinforcer for gel formation under visible light in a one pot process. EG together with water was used as a co-solvent to enhance dispersibility of g-CN. The EG-containing hybrid gels could be transformed into hydrogels *via* simple solvent exchange. Both types of networks show remarkable storage moduli (up to 650 kPa for hybrid gels and 720 kPa for hydrogels) and compression moduli (up to 9.45 MPa for gels and 3.45 MPa for hydrogels), *i.e.* are of the order of cartilage or tendon. Cyclic compression tests of both gels and hydrogels after 20 consecutive cyclic compressions state recovery of the initial state without energy loss. Moreover, application of spatially controlled optical patterning was investigated *via* simple, home-made photomasks. The present work is to our opinion an important step in the design of reinforced hydrogel materials with significant mechanical properties *via* a new and facile approach for advanced applications such as medical coatings, fillers and cartilage or tendon implants, photocatalytic products, or the synthesis of hydrogels in additive manufacturing technologies.

Conflicts of interest

There are no conflicts of interest to declare.

Acknowledgements

The authors thank Max Planck Society for financial support, Dr Kerstin Blank and Dr Alberto Sanz de Leon for rheometer access and Ms Katharina Otte for organizational support. Open Access funding provided by the Max Planck Society.

Notes and references

1 E. A. Appel, X. J. Loh, S. T. Jones, F. Biedermann, C. A. Dreiss and O. A. Scherman, *J. Am. Chem. Soc.*, 2012, **134**, 11767–11773.
2 J. Zhu and R. E. Marchant, *Expert Rev. Med. Devices*, 2011, **8**, 607–626.
3 S. Yodmuang, S. L. McNamara, A. B. Nover, B. B. Mandal, M. Agarwal, T. A. Kelly, P. H. Chao, C. Hung, D. L. Kaplan and G. Vunjak-Novakovic, *Acta Biomater.*, 2015, **11**, 27–36.
4 J. L. Drury and D. J. Mooney, *Biomaterials*, 2003, **24**, 4337–4351.
5 K. T. Nguyen and J. L. West, *Biomaterials*, 2002, **23**, 4307–4314.
6 Y. Qiu and K. Park, *Adv. Drug Delivery Rev.*, 2001, **53**, 321–339.
7 T. R. Hoare and D. S. Kohane, *Polymer*, 2008, **49**, 1993–2007.
8 H. Yuk, S. Lin, C. Ma, M. Takaffoli, N. X. Fang and X. Zhao, *Nat. Commun.*, 2017, **8**, 14230.
9 X. Dai, Y. Zhang, L. Gao, T. Bai, W. Wang, Y. Cui and W. Liu, *Adv. Mater.*, 2015, **27**, 3566–3571.
10 L. Li, B. Yan, J. Yang, W. Huang, L. Chen and H. Zeng, *ACS Appl. Mater. Interfaces*, 2017, **9**, 9221–9225.
11 S. K. Mujumdar and R. A. Siegel, *J. Polym. Sci., Part A: Polym. Chem.*, 2008, **46**, 6630–6640.
12 Q. Chen, H. Chen, L. Zhu and J. Zheng, *J. Mater. Chem. B*, 2015, **3**, 3654–3676.
13 A. Nakayama, A. Kakugo, J. P. Gong, Y. Osada, M. Takai, T. Erata and S. Kawano, *Adv. Funct. Mater.*, 2004, **14**, 1124–1128.
14 B. G. Cooper, R. C. Stewart, D. Burstein, B. D. Snyder and M. W. Grinstaff, *Angew. Chem., Int. Ed.*, 2016, **55**, 4226–4230.
15 A. Agrawal, N. Rahbar and P. D. Calvert, *Acta Biomater.*, 2013, **9**, 5313–5318.
16 M. Fukasawa, T. Sakai, U.-i. Chung and K. Haraguchi, *Macromolecules*, 2010, **43**, 4370–4378.
17 D. E. Fullenkamp, L. He, D. G. Barrett, W. R. Burghardt and P. B. Messersmith, *Macromolecules*, 2013, **46**, 1167–1174.
18 S. E. Bakarich, R. Gorkin, 3rd, M. in het Panhuis and G. M. Spinks, *ACS Appl. Mater. Interfaces*, 2014, **6**, 15998–16006.
19 A. Bin Imran, K. Esaki, H. Gotoh, T. Seki, K. Ito, Y. Sakai and Y. Takeoka, *Nat. Commun.*, 2014, **5**, 5124.
20 T. Murakami, B. V. K. J. Schmidt, H. R. Brown and C. J. Hawker, *Macromolecules*, 2015, **48**, 7774–7781.
21 Y. Liu, M. Zhu, X. Liu, W. Zhang, B. Sun, Y. Chen and H.-J. P. Adler, *Polymer*, 2006, **47**, 1–5.
22 O. Okay and W. Oppermann, *Macromolecules*, 2007, **40**, 3378–3387.
23 J. Yang, C.-R. Han, X.-M. Zhang, F. Xu and R.-C. Sun, *Macromolecules*, 2014, **47**, 4077–4086.
24 J. Djonlagic, A. Lancuski, M. S. Nikolic, J. Rogan, S. Ostojic and Z. Petrovic, *J. Appl. Polym. Sci.*, 2017, **134**, 44535.
25 M. Liu, Y. Ishida, Y. Ebina, T. Sasaki, T. Hikima, M. Takata and T. Aida, *Nature*, 2015, **517**, 68–72.
26 J. Sun, B. V. K. J. Schmidt, X. Wang and M. Shalom, *ACS Appl. Mater. Interfaces*, 2017, **9**, 2029–2034.
27 B. Kumru, M. Shalom, M. Antonietti and B. V. K. J. Schmidt, *Macromolecules*, 2017, **50**, 1862–1869.
28 G. Algara-Siller, N. Severin, S. Y. Chong, T. Bjorkman, R. G. Palgrave, A. Laybourn, M. Antonietti, Y. Z. Khimyak, A. V. Krasheninnikov, J. P. Rabe, U. Kaiser, A. I. Cooper, A. Thomas and M. J. Bojdys, *Angew. Chem., Int. Ed.*, 2014, **53**, 7450–7455.
29 K. Schwinghammer, B. Tuffy, M. B. Mesch, E. Wirnhier, C. Martineau, F. Taulelle, W. Schnick, J. Senker and B. V. Lotsch, *Angew. Chem., Int. Ed.*, 2013, **52**, 2435–2439.
30 X. Wang, K. Maeda, A. Thomas, K. Takanabe, G. Xin, J. M. Carlsson, K. Domen and M. Antonietti, *Nat. Mater.*, 2009, **8**, 76–80.
31 J. Liu, H. Wang and M. Antonietti, *Chem. Soc. Rev.*, 2016, **45**, 2308–2326.
32 B. Kumru, M. Antonietti and B. V. K. J. Schmidt, *Langmuir*, 2017, **33**, 9897–9906.
33 J. Ji, J. Wen, Y. Shen, Y. Lv, Y. Chen, S. Liu, H. Ma and Y. Zhang, *J. Am. Chem. Soc.*, 2017, **139**, 11698–11701.

Open Access Article. Published on 13 March 2018. Downloaded on 7/23/2025 12:29:56 PM.
This article is licensed under a Creative Commons Attribution 3.0 Unported Licence.

34 Q. Han, B. Wang, Y. Zhao, C. Hu and L. Qu, *Angew. Chem., Int. Ed.*, 2015, **54**, 11433–11437.
35 J. Liu, Y. Liu, N. Liu, Y. Han, X. Zhang, H. Huang, Y. Lifshitz, S.-T. Lee, J. Zhong and Z. Kang, *Science*, 2015, **347**, 970–974.
36 R. Kuriki, K. Sekizawa, O. Ishitani and K. Maeda, *Angew. Chem., Int. Ed.*, 2015, **54**, 2406–2409.
37 J. Lin, Z. Pan and X. Wang, *ACS Sustainable Chem. Eng.*, 2014, **2**, 353–358.
38 K. K. Datta, B. V. Reddy, K. Ariga and A. Vinu, *Angew. Chem., Int. Ed.*, 2010, **49**, 5961–5965.
39 F. Su, S. C. Mathew, L. Mohlmann, M. Antonietti, X. Wang and S. Blechert, *Angew. Chem., Int. Ed.*, 2011, **50**, 657–660.
40 J. Xu and M. Antonietti, *J. Am. Chem. Soc.*, 2017, **139**, 6026–6029.
41 S. Dadashi-Silab, M. A. Tasdelen, B. Kiskan, X. Wang, M. Antonietti and Y. Yagci, *Macromol. Chem. Phys.*, 2014, **215**, 675–681.
42 B. Kiskan, J. Zhang, X. Wang, M. Antonietti and Y. Yagci, *ACS Macro Lett.*, 2012, **1**, 546–549.
43 J. Poostforooshan, A. Badiei, M. Kolahdouz and A. P. Weber, *ACS Appl. Mater. Interfaces*, 2016, **8**, 21731–21741.
44 J. Liu, T. An, Z. Chen, Z. Wang, H. Zhou, T. Fan, D. Zhang and M. Antonietti, *J. Mater. Chem. A*, 2017, **5**, 8933–8938.
45 Y. Zhang, Z. Zhou, Y. Shen, Q. Zhou, J. Wang, A. Liu, S. Liu and Y. Zhang, *ACS Nano*, 2016, **10**, 9036–9043.
46 J. Yan, M.-T. F. Rodrigues, Z. Song, H. Li, H. Xu, H. Liu, J. Wu, Y. Xu, Y. Song, Y. Liu, P. Yu, W. Yang, R. Vajtai, H. Li, S. Yuan and P. M. Ajayan, *Adv. Funct. Mater.*, 2017, **27**, 1700653.
47 J. W. Ko, W. S. Choi, J. Kim, S. K. Kuk, S. H. Lee and C. B. Park, *Biomacromolecules*, 2017, **18**, 3551–3556.
48 E. G. Gillan, *Chem. Mater.*, 2000, **12**, 3906–3912.
49 M. Shalom, S. Inal, C. Fettkenhauer, D. Neher and M. Antonietti, *J. Am. Chem. Soc.*, 2013, **135**, 7118–7121.
50 N. Wang, H. Fan, J. Sun, Z. Han, J. Dong and S. Ai, *Carbon*, 2016, **109**, 141–148.
51 G. Peng, L. Xing, J. Barrio, M. Volokh and M. Shalom, *Angew. Chem., Int. Ed.*, 2018, **57**, 1186–1192.
52 C. Huang, C. Chen, X. Ye, W. Ye, J. Hu, C. Xu and X. Qiu, *J. Mater. Chem. A*, 2013, **1**, 12192.
53 X. She, H. Xu, Y. Xu, J. Yan, J. Xia, L. Xu, Y. Song, Y. Jiang, Q. Zhang and H. Li, *J. Mater. Chem. A*, 2014, **2**, 2563–2570.
54 H. Ju, F. Zhu, H. Xing, Z. L. Wu and F. Huang, *Macromol. Rapid Commun.*, 2017, **38**, 1700232.
55 K. Numata, N. Ifuku, H. Masunaga, T. Hikima and T. Sakai, *Biomacromolecules*, 2017, **18**, 1937–1946.
56 A. Thorvaldsson, J. Silva-Correia, J. M. Oliveira, R. L. Reis, P. Gatenholm and P. Walkenström, *J. Appl. Polym. Sci.*, 2013, **128**, 1158–1163.
57 M. Kheirabadi, R. Bagheri and K. Kabiri, *Polym. Bull.*, 2015, **72**, 1663–1681.
58 E. Zhang, T. Wang, C. Lian, W. Sun, X. Liu and Z. Tong, *Carbon*, 2013, **62**, 117–126.
59 M. Liu, W. Li, J. Rong and C. Zhou, *Colloid Polym. Sci.*, 2012, **290**, 895–905.
60 M. Liu, Y. Zhang, J. Li and C. Zhou, *Int. J. Biol. Macromol.*, 2013, **58**, 23–30.
61 Q. Rong, W. Lei, L. Chen, Y. Yin, J. Zhou and M. Liu, *Angew. Chem., Int. Ed.*, 2017, **56**, 14159–14163.
62 E. C. Muniz and G. Geuskens, *Macromolecules*, 2001, **34**, 4480–4484.
63 Q. Wang, R. Hou, Y. Cheng and J. Fu, *Soft Matter*, 2012, **8**, 6048.
64 W. Li, D. Wang, W. Yang and Y. Song, *RSC Adv.*, 2016, **6**, 20166–20172.
65 W. Huang, J. Shen, N. Li and M. Ye, *Polym. Eng. Sci.*, 2015, **55**, 1361–1366.
66 S. C. Yan, Z. S. Li and Z. G. Zou, *Langmuir*, 2009, **25**, 10397–10401.
67 Q. T. Nguyen, Y. Hwang, A. C. Chen, S. Varghese and R. L. Sah, *Biomaterials*, 2012, **33**, 6682–6690.
68 S. Bhat, L. Lidgren and A. Kumar, *Macromol. Biosci.*, 2013, **13**, 827–837.

 This journal is © The Royal Society of Chemistry 2018